Desalination and Water Treatment
www.deswater.com

doi: 10.1080/19443994.2015.1043494

57 (2016) 10101–10110
May

Taylor & Francis
Taylor & Francis Group

Experiment and modeling for performance of a spiral-wound pressure-retarded osmosis membrane module

Sungyun Lee[a], Yu Chang Kim[a,b,*], Sang-Jin Park[a], Sook-Kyung Lee[c], Hyu-Chang Choi[c]

[a]*Department of Extreme Thermal Systems, Korea Institute of Machinery and Materials, Daejeon 305-343, Korea, Tel. +82 42 868 7397; Fax: +82 42 868 7355; email: kimyc@kimm.re.kr (Y.C. Kim)*
[b]*Environment & Energy Mechanical Engineering, University of Science & Technology, Daejeon 305-350, Korea*
[c]*KHNP-Central Research Institute, Daejeon 305-343, Korea*

Received 15 January 2015; Accepted 15 April 2015

ABSTRACT

Pressure-retarded osmosis (PRO) process utilizes the transport of water through a semipermeable membrane to generate electricity from salinity gradient resources. Recent PRO research has shown the feasibility of PRO technologies in laboratory-scale experiments, but there is currently a lack of experimental pilot-scale investigations to ensure the success of PRO technology. This study was conducted to predict the power density of a PRO module using PRO membrane transport properties such as water permeability, salt permeability, and membrane structure parameter. The performance of an 8040 spiral-wound PRO module was experimentally investigated, and the results were compared with the simulated prediction. The maximum power density of the investigated PRO module was 1.8 W m^{-2} at 10.4 bar using 35 g L^{-1} of NaCl as a draw solution. At the outlet of the module, the concentration changes of the draw and feed solutions were observed, suggesting a gradual decrease of membrane power density inside the PRO module. The simulation model, which considered concentration changes of draw and feed solutions, reverse salt flux, and mass transport coefficient inside the module, closely estimated the performance of the PRO module. However, the model overestimated the power density at high hydraulic pressure difference. It was concluded that severe increase of reverse salt flux at a high hydraulic pressure difference negatively contributed to the performance of the PRO module.

Keywords: Spiral-wound module; Pressure-retarded osmosis; Power density; Modeling

1. Introduction

Recently, high oil energy costs and issues such as climate change have motivated research in renewable energy resources. Among the multitude of renewable energy technologies, pressure-retarded osmosis (PRO) technology has been recognized as a feasible technology to utilize salinity gradient energy [1–3]. It has been reported that global renewable energy from salinity gradients in the estuaries is approximately 2 TW, which accounts for 13% of world energy consumption [4,5]. PRO process utilizes osmosis to transport water through a semipermeable membrane to generate

*Corresponding author.

Presented at GMVP Desalination Academic Workshop, Seoul, Korea, December 9, 2014

electricity. Thus, a high-performance PRO membrane is essential in implementing the technology.

A power density of 5 W m^{-2} was suggested as a technical barrier for making PRO economically feasible [6]. Since the first experimental PRO test in 1976 by Loeb [7], the power density of membranes has been improved, thanks to the efforts of many researchers. For example, 1.5 W m^{-2} of power density was obtained in 1981 using the osmotic differential of seawater and freshwater [1]. Recently, 5.7 W m^{-2} of power density was achieved under similar osmotic differential using a thin-film composite hollow fiber membrane. An even higher power density of 10.6 W m^{-2} was obtained using seawater brine (1 M NaCl) [8]. Straub et al. [9] reported power densities of 7.5, 14.1, 39.4, and 59.7 W m^{-2} using 0.6, 1, 2, and, 3 M NaCl draw solutions, respectively, by using a commercial flat-sheet thin-film composite FO membrane.

Although some PRO membranes seem to meet the 5 W m^{-2} target, most of these studies only investigated PRO membranes in a laboratory-scale. As a result, there is currently a lack of experimental pilot-scale investigations to ensure the success of PRO technology [10]. Statkraft, a Norwegian state owned electricity company, conducted the first prototype PRO test in 2009 to harvest 10 kW of salinity power from seawater and brackish lake water [10,11]. The Mega-ton Water System project in Japan also investigated a pilot-scale PRO system to utilize brine from a reverse osmosis process and treated effluent from a wastewater treatment plant [12]. They reported that their PRO hollow fiber membrane module could obtain 4.4 W m^{-2}. However, the detailed experimental results from Statkraft and the Mega-ton Water System projects are inconclusive. Kim et al. [13] experimentally tested a prototype spiral-wound PRO module using seawater and tap water. They obtained 1.0 W m^{-2} of maximum power density and noted reduced osmotic water permeation due to the shadow effect by the spacer of the module. In addition to the apparent power density of PRO membrane, net power generation by PRO system should be considered for the implementation of PRO technology. The net power generation depends on various factors such as efficiency of energy conversion devices, PRO system design [14], draw to permeate flow ratio [15,16], and feed recovery [17].

The performance PRO membranes are affected by experimental conditions including the concentration of the draw and feed solutions, flow rate, and temperature [2,13,18,19]. Therefore, a modeling equation is required to predict the power density of PRO membranes under various conditions. Yip et al. [20] incorporated external concentration polarization (ECP), internal concentration polarization (ICP), and reverse salt flux into water flux in PRO mode to predict the performance of the PRO membrane. The model uses membrane transport parameter and hydraulic conditions including water permeability (A), salt permeability (B), membrane structure parameter (S), and mass transport coefficient (k). The equation has been widely accepted by many researchers, and the effectiveness has been proved and provided inspiration for PRO membrane development [21–25]. However, additional considerations are required to predict PRO module performance from laboratory-scale test results. For example, in the laboratory-scale test, the change of the draw and feed concentration is negligible due to the relatively small permeate flow rate of PRO coupons compared to the draw and feed flow rate. In the module-scale, the concentration of the draw and feed solution changes considerably along the flow direction. The concentration of the draw solution is diluted, and the concentration of the feed solution increases by water permeate flux. Thus, the power density of the PRO membrane module is lower than that of a laboratory-scale PRO membrane.

This study was conducted to predict the power density of a PRO module from PRO membrane transport parameters. We experimentally investigated the performance of an 8040 spiral-wound membrane using a draw solution of 35,000 mg L^{-1} NaCl and freshwater. The results were then compared with simulations in regard to the concentration change of the draw and feed solutions, reverse salt flux, and the mass transport coefficient inside the module. The results can be applied to estimate PRO module performance and PRO membrane development.

2. Material and methods

2.1. Water flux in the PRO module and modeling

The water permeability (A) and salt permeability (B) of the PRO module were measured by an RO experiment using 6,000 mg L^{-1} of NaCl solution at 13 bar. The A value and B value of the PRO module were calculated using Eqs. (1) and (2).

$$J_w = A(\Delta P - \Delta\pi) \tag{1}$$

$$B = \frac{J_w(1-R)}{R}\exp\left(-\frac{J_w}{k}\right) \tag{2}$$

where R is the salt rejection of the module, and J_w is water flux. The mass transfer coefficient (k) is determined by [17]

$$k = \frac{\mathrm{Sh}D}{d_\mathrm{h}} \tag{3}$$

where Sh is the Sherwood number, D is the diffusion coefficient of the NaCl, and d_h is the hydraulic diameter.

$$\mathrm{Sh} = 0.2\ \mathrm{Re}^{0.57}\ \mathrm{Sc}^{0.40} \tag{4}$$

The solute resistivity to salt transport in porous substrate K_R, which is a function of the structural parameter S and D ($K_\mathrm{R} = \frac{S}{D}$), was calculated using Eq. (5) [2] from water flux in the PRO experiment.

$$J_\mathrm{w} = A\left[\frac{\pi_{\mathrm{D,b}}\ \exp\left(-\frac{J_\mathrm{w}}{k}\right) - \pi_{\mathrm{F,b}}\ \exp(J_\mathrm{w}K_\mathrm{R})}{1 + \frac{B}{J_\mathrm{w}}\left[\exp(J_\mathrm{w}K_\mathrm{R}) - \exp\left(-\frac{J_\mathrm{w}}{k}\right)\right]} - \Delta P\right] \tag{5}$$

The power density (W) of the PRO membrane module was calculated using the product of J_w and ΔP [1]:

$$W = J_\mathrm{w}\Delta P \tag{6}$$

The increase of the water flow rate and velocity of the draw solution in the module due to the water flux from the feed solution were determined using Eqs. (7) and (8).

$$Q_{D,i+1} = Q_{D,i} + J_i\Delta A_\mathrm{m} \tag{7}$$

$$U_{D,i} = \frac{Q_{D,i}}{A_\mathrm{c}\varepsilon} \tag{8}$$

where ΔA_m is a segment of the membrane area divided along the length of the PRO module, Q_i, J_i, and U_i represent water flow rate, water flux, and water velocity at the i-th segments of the membrane area, respectively. A_c and ε (=0.8) are a cross section area and spacer voidage of the draw channel, respectively. Similarly, the decrease of water flow rate of the feed solution due to the water flux through membrane can be obtained using the following formula:

$$Q_{F,i+1} = Q_{F,i} - J_i\Delta A_\mathrm{m} \tag{9}$$

The concentration changes of the draw and feed solutions were calculated by Eqs. (10–12).

$$C_{D,b,i+1} = \frac{C_{D,b,i}\ Q_{D,i} - B(C_{D,m,i} - C_{F,m,i})\Delta A_\mathrm{m}}{Q_{D,i+1}} \tag{10}$$

$$C_{F,b,i+1} = \frac{C_{F,b,i}Q_{F,i} + B(C_{D,m,i} - C_{F,m,i})\Delta A_\mathrm{m}}{Q_{F,i+1}} \tag{11}$$

$$C_{D,m,i} - C_{F,m,i} = \frac{C_{D,b,i}\ \exp\left(-\frac{J_\mathrm{w}}{k}\right) - C_{F,b,i}\ \exp(J_w K_\mathrm{R})}{1 + \frac{B}{J_\mathrm{w}}\left[\exp(J_\mathrm{w}K_\mathrm{R}) - \exp\left(-\frac{J_\mathrm{w}}{k}\right)\right]} \tag{12}$$

The flow behaviors and concentrations for the draw and feed solutions inside the module can be obtained using the equations described above. Here, we simplified the water flow paths as a plate-and-frame module. The total reverse salt flux of the module can be determined using water flow rate and concentration at the inlet and outlet of the module by

$$J_\mathrm{s} = \frac{Q_{F,\mathrm{out}}C_{F,b,\mathrm{out}} - Q_{F,\mathrm{in}}C_{F,b,\mathrm{in}}}{A_\mathrm{m}} \tag{13}$$

where A_m is PRO total membrane area of the module.

2.2. Pilot system

Fig. 1 shows a schematic diagram of the pilot-scale PRO experimental unit. A high-pressure pump (CRN 10-14, Grundfos, Denmark) and two low-pressure pumps (draw: CRN 1-9; feed: CRN 10-3, Grundfos, Denmark) were installed for circulation of the draw and feed solutions. The hydraulic pressure and flow rate of the draw solution side were controlled using a back-pressure valve and a variable-frequency drive (VFD) for the high-pressure and low-pressure pump. Since less hydraulic pressure on the feed side is desirable for a higher net power density of the PRO system [17], the feed solution flow rate was controlled using only the VFD of the feed side low-pressure pump to minimize the inlet pressure. VFDs are commonly used to modify motor speed. They can, however, generate noise in the system cable. If the noise caused by high frequency energy is not insulated, it can interfere with equipment and units such as conductivity, pressure, and flow transmitters. The insulation of VFD noise and the condition of monitoring instruments were checked prior to the experiment. Pressure, flow rate, concentration, and temperature were monitored using pressure transmitters (T2000, LEFOO, China), magnetic flow meters (feed side: model SAD-25/SAZ-3,

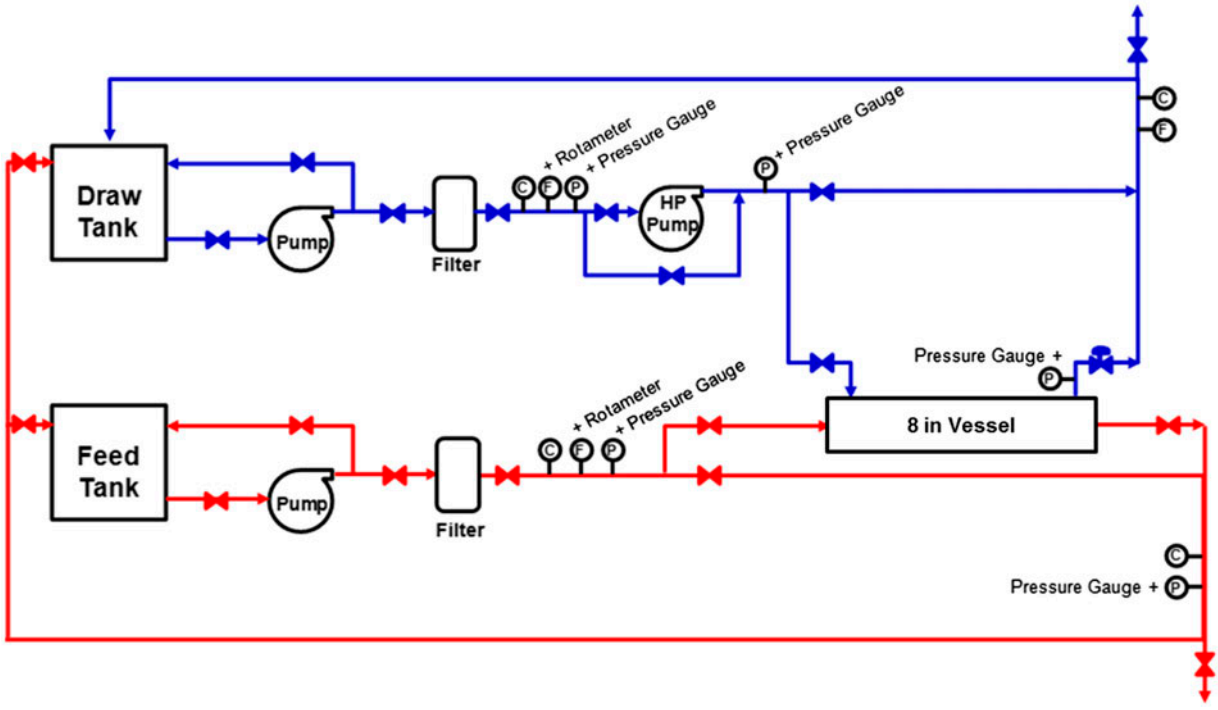

Fig. 1. Schematic diagram of the 8040 spiral-wound PRO module experimental setup.

draw side: model SDA-40/SAZ-3, SATC, Korea), conductivity meters (Signet, US), and temperature meters (RCH-1, Lumix, Korea) in the pipeline or tank. The conductivity meters were calibrated before the experiment for accurate conversion of conductivity to concentration. The operation data were collected every 10 s. The temperature of the each tank was adjusted using a temperature controller. Bypass lines were installed for calibration of the feed and draw solution flow meters.

2.3. 8040 PRO module and experiment conditions

The 8040 PRO module was provided by Toray Chemical Korea (previously Woongjin Chemical Co., Korea). The 8040 PRO module is the same size as the 8040 reverse osmosis module and is 0.2 m (8 in.) in diameter and 1 m (40 in.) in length. The PRO module has 17.9 m^2 of membrane (A_m) with a polyamide coating. According to the manufacturer, a special spacer for the feed solution was applied to reduce the pressure resistance of the feed channel. The draw channel spacer has 0.8 mm (32 mil.) of thickness, and the cross section area of the draw channel (A_c) is 97 cm^2. The feed solution flowed outside of the membrane envelop facing the rejection layer of the membrane, and the draw solution flowed inside of the membrane envelop facing the support layer of the membrane. For PRO experiments, the draw and feed solutions were introduced to the module in the co-current direction at 25 and 7 LPM, respectively. 35 g L^{-1} of NaCl was used for the draw solution, and tap water (140 mg L^{-1}) was used for the feed solution. Each solution was recirculated to each tank, and the concentrations of both solutions did not undergo any significant changes during the PRO experiment due to the large volume of the tanks (3 m^3). To determine the membrane transport properties, the PRO module was operated in RO mode using 6,000 mg L^{-1} of NaCl solution at 13 bar. The flow rate and the mass transport (k) for the RO experiment was 27 LPM and 4.43×10^{-5} m s^{-1}, respectively.

3. Results and discussion

3.1. Calibration of flow meters

Accurate measurement of flow rate is important in estimating the performance of the PRO module. Even the same model of flow meters can provide a different value due to electrical noise in the pilot system caused by VFD. If the error is not significantly noticeable, the measurement error can be overlooked, and the result can mislead PRO performance. For example, a 0.5 LPM error of measurement at 11 bar corresponds

with 0.5 W m^{-2} for the 8040 PRO module with 17.9 m^2 of membrane. The difference in the flow meter value of the inlet and outlet of the vessel was monitored using a bypass line which allows the same flow rate for both the inlet and outlet of the vessel. The flow rate difference measured by the flow meters increased in conjunction with flow rate. The inlet flow rate was calibrated using the relationship (Fig. 2), and PRO module performance was evaluated accurately.

3.2. Performance of the spiral-wound PRO module

Fig. 3 shows the performance of the 8040 PRO module at different hydraulic pressures in accordance with time. Hydraulic pressure difference was increased from 4 to 20 bar in 4 bar increments and then decreased to 4 bar in 4 bar decrements. As hydraulic pressure difference was increased, PRO flux decreased and water flux was recovered when applied hydraulic pressure was decreased. The PRO module was then operated at 8 bar ΔP to confirm stable performance of the module. The PRO module showed stable performance at the tested hydraulic pressure difference range. When 20 bar was applied, flux was negative, which means water was transported from the draw solution side to the feed solution side similar to a reverse osmosis process. Here, it is worthwhile to note that the osmotic pressure difference of the solutions (26 bar) was higher than the hydraulic pressure difference (20 bar) ($\Delta\pi > \Delta P$). It is considered that the low salt selectivity of the PRO membrane could cause a less effective osmotic pressure difference across the membrane.

Flux and power density of the PRO module at applied pressure are depicted in Fig. 4. Without hydraulic pressure, the module had 11.76 $Lm^{-2}\,h^{-1}$. According to the flux trend as a function of hydraulic pressure, no flux is expected at 18.8 bar of ΔP. The power density showed a parabolic trend in terms of hydraulic pressure, which is similar to the laboratory-scale PRO studies [17,24,26,27]. The maximum power density of the investigated PRO module was 1.77 W m^{-2} at 10.4 bar using 35 g L^{-1} of NaCl as a draw solution.

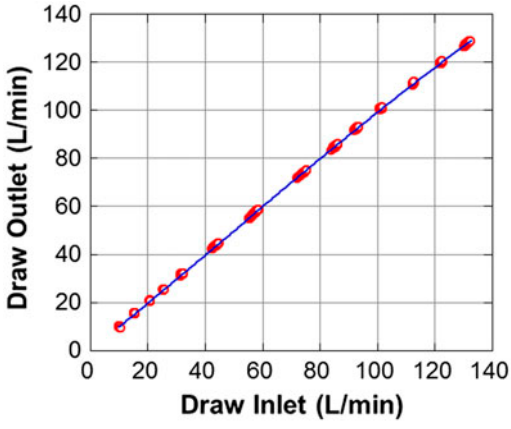

Fig. 2. Calibration of flow meter for draw solution using a bypass pipe.

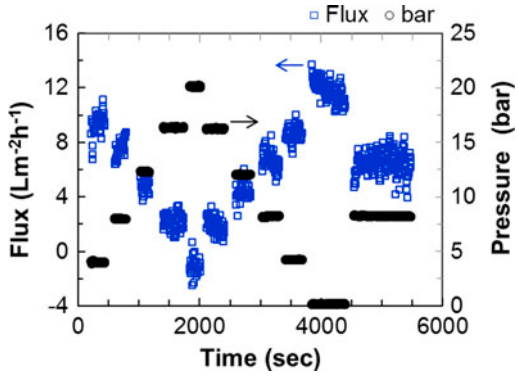

Fig. 3. Effect of the hydraulic pressure difference (ΔP) on the water flux of the 8040 PRO module with time.
Notes: The draw and feed solutions were 35,000 mg L^{-1} NaCl and tap water (140 mg L^{-1}), respectively. The inlet flow rates of draw and feed solutions were maintained at 25 and 7 LPM, respectively.

Water is transported across the membrane from the feed solution to the draw solution due to osmotic pressure difference. Thus, the draw solution could be diluted, and the feed solution could be concentrated in the PRO module. At the same time, slats diffuse in the opposite direction of water transport so that feed concentration could increase more than the volume reduction effect. Fig. 5 shows the concentration of both the feed and draw solution at the inlet and outlet of the PRO module. As a result of higher water flux at lower hydraulic pressure difference, the draw solution was more diluted at a lower hydraulic pressure difference. However, the opposite trend was observed for the feed solution considering water flux; a higher increase of feed solution concentration at the higher hydraulic pressure difference was observed even though there was lower water flux. This higher increase of feed concentration at higher concentration is described in Section 3.4. These concentration changes of draw and feed solutions suggest a gradual decrease of membrane power density in the spiral-wound PRO module. Therefore, dilution of draw solution, concentration of feed solution, and reverse salt diffusion should be considered to estimate the performance of the PRO module from a laboratory-scale PRO membrane test.

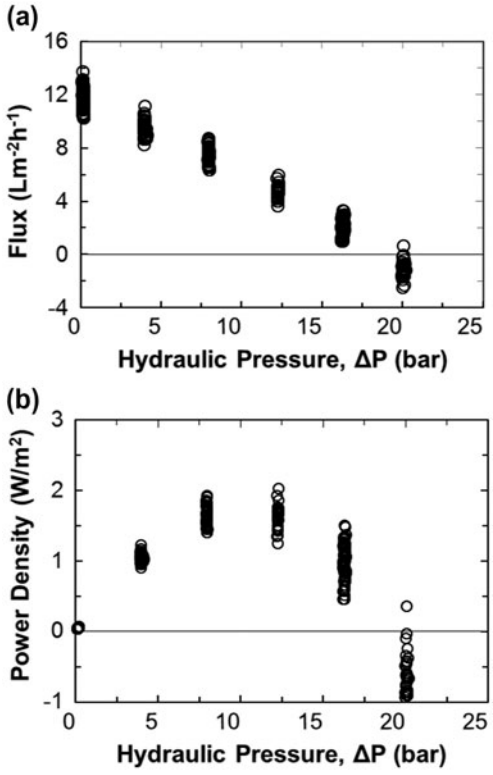

Fig. 4. Experimental water flux (a) and corresponding projected power density (b) of the PRO module as a function of hydraulic pressure difference (ΔP).
Note: The data before 2,000 s in Fig. 3 were used to minimize the effect of inlet concentration changes in draw and feed solutions.

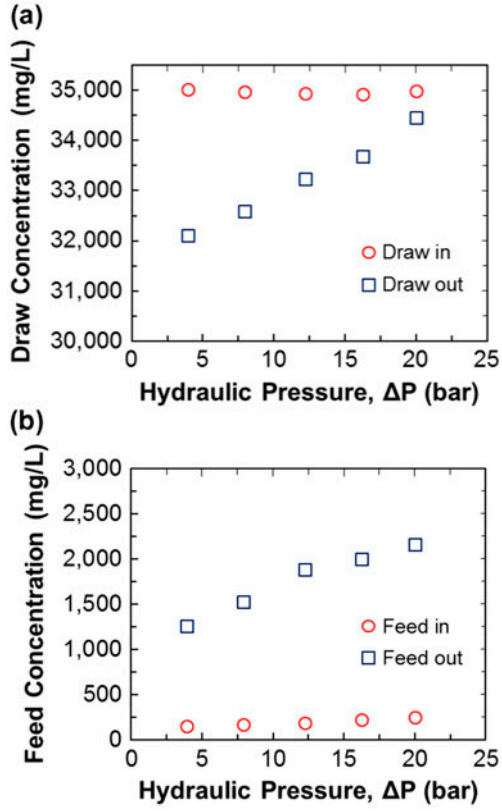

Fig. 5. Concentrations of the draw solution (a) and feed solution (b) at inlet and outlet of the PRO module as a function of hydraulic pressure difference (ΔP).
Note: The draw and feed solutions were 35,000 mg L^{-1} NaCl and tap water (140 mg L^{-1}), respectively.

3.3. PRO membrane transport parameters for performance modeling

Water permeability (A), salt permeability (B), and membrane structure parameter (S) were used to predict the power density of the PRO membrane [4,17,22]. A and B values can be obtained from the RO experiment using Eqs. (1) and (2). The RO experiment was conducted at various temperatures in order to investigate the effect of temperature on A and B values. The water flux in RO mode increased as an increase in temperature, but the removal efficiency was a constant 95% at the tested temperature range. Fig. 6 shows the effect of temperature on water permeability and salt permeability. Water permeability increased 12.7% from 15 to 20˚C; A value was 2.08 and 2.34 $Lm^{-2}\,h^{-1}\,bar^{-1}$ at 15 and 20˚C, respectively. Water permeability and temperature had relationship, $J_T = J_{20^\circ C} \times \exp[0.0225 \times (T - 20)]$. The exponential constant was similar to the previous study [28], 0.0239, which investigated the effect of temperature on the performance of forward osmosis membranes made of cellulose triacetate. Salt permeability also increased as temperature increased. Salt permeability increased 10% from 15 to 20˚C; B was 0.73 and 0.80 $Lm^{-2}\,h^{-1}$ at 15 and 20˚C, respectively. The relationship between B and temperature was $B_T = 0.5372 \times \exp(0.0202 \times T)$. Since water permeability and salt permeability are both dependent on temperature, the power density of the PRO membrane is also temperature dependent [25,26,29]. For example, She et al. [26] found improved maximum power density from 3.8 to 5.1 W m^{-2} when the temperature increased from 25 to 35˚C. Similar results were also observed by Anastasio et al. They showed an improvement of peak power density from 1.3 W m^{-2} at 20˚C to 4.0 W m^{-2} at 40˚C. The improvement of power density could be a dominant effect of A value on water flux [26]. Since the PRO membrane module performance test was conducted at 25˚C, we used 2.63 and 0.89 $Lm^{-2}\,h^{-1}$ for A and B estimated from the relationship with temperature. The PRO membrane was a thin-film composite membrane that had a polysulfone-based support layer with a

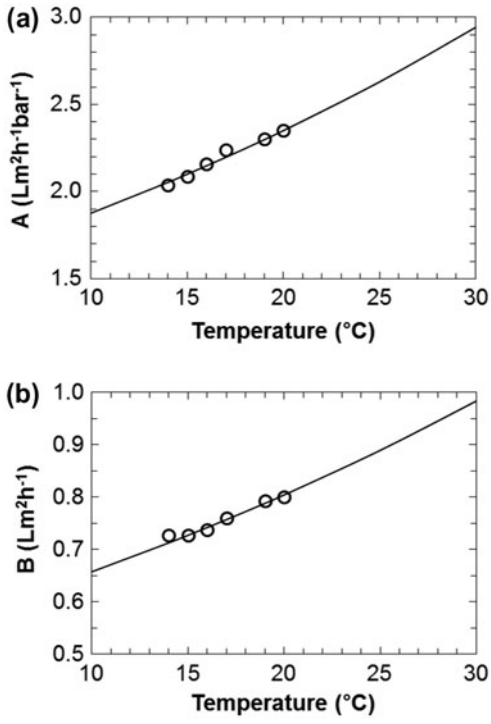

Fig. 6. Effect of temperature on water permeability coefficient (A) (a) and salt permeability coefficient (B) (b) of the PRO module.
Note: Both A and B were measured in RO experiments at 13 bar.

sponge-like structure. As a result of having the same support layer in our previous study, the membrane structure parameter was taken from the literature [21]. The membrane structure parameter of 1,645 μm at 10 bar was used for simulation of the PRO membrane performance.

3.4. Estimation of PRO module performance

As previously described, the concentration of the draw solution gradually decreases as it flows inside the module due to dilution by water flux. At the same time, the concentration of the feed solution becomes concentrated due to volume reduction. As a result of the volume changes of the draw and feed solutions, the transport conditions including flow velocity and mass transport coefficient also change affecting ECP and ICP on the membrane surface. Using Eqs. (3)–(12), these changes were considered for simulation of the PRO module performance. Fig. 7 shows the simulated concentrations and performance distributions inside the PRO module at 4 and 8 bar hydraulic pressure difference. The decrease of concentration difference between draw and feed concentrations negatively contributed to the water flux and power density along the module length. The model closely estimated the outlet concentration of draw solution at 4 and 8 bar. However, the simulated feed concentrations at the outlet of the module were lower than the experimentally measured value).

Although there was an underestimation of the concentration of feed solution at the outlet, our approach (model 3) showed favorable agreement with the experimentally measured maximum power density compared to model 1 and model 2 (Fig. 8). Model 1 represents a laboratory-scale simulation where changes of experimental conditions are negligible. Model 1 used a hydraulic transport condition from a previous study as a representative laboratory-scale test condition [21]. The size of the test cell was 26 mm wide × 77 mm long × 1.5 mm deep, and the draw solution flow rate was 0.5 LPM (flow velocity of 26 cm s^{-1}) which corresponded to a mass transfer coefficient of 9.68×10^{-5} m s^{-1}. Model 2 also did not consider the changes of conditions in the module like module 1, but it applied the initial inlet draw flow rate of the PRO module. The flow rate of the draw solution for the PRO module was 25 LPM (flow velocity of 5.4 cm s^{-1}) which corresponded to a mass transfer coefficient of 4.67×10^{-5} m s^{-1}. Since the mass transfer coefficient affects dilutive ECP as $\exp(-J_w/k)$, the smaller mass transfer coefficient of the PRO module can negatively contribute to the power density. Model 3 applied the updated conditions including draw and feed concentrations and the mass transfer coefficient inside the PRO module to estimate performance.

Compared to the experimental maximum power density, model 1 and model 2 significantly overestimated maximum power density of the PRO module by as much as 34 and 28%, respectively (Fig. 8). A minor difference of maximum power density was obtained between model 1 and model 2 at the simulation conditions. If the salt permeability is negligible ($B \approx 0$), the dilutive ECP factor, $\exp(-J_w/k)$ was estimated at 0.98 and 0.96 for model 1 and model 2, respectively. An ECP factor value close to 1 means that ECP has less of an effect on the PRO performance. This indicates that the effect of ECP with relatively small water flux (J_w) at a hydraulic pressure difference of maximum power density and a mass transport coefficient difference less than one order could not account for the power density reduction of the experimental module performance.

Model 3 closely estimated flux and power density at below 8 bar of hydraulic pressure difference. Thus, this shows that a consideration of concentration changes in the draw and feed solutions in the module is important in predicting the PRO module

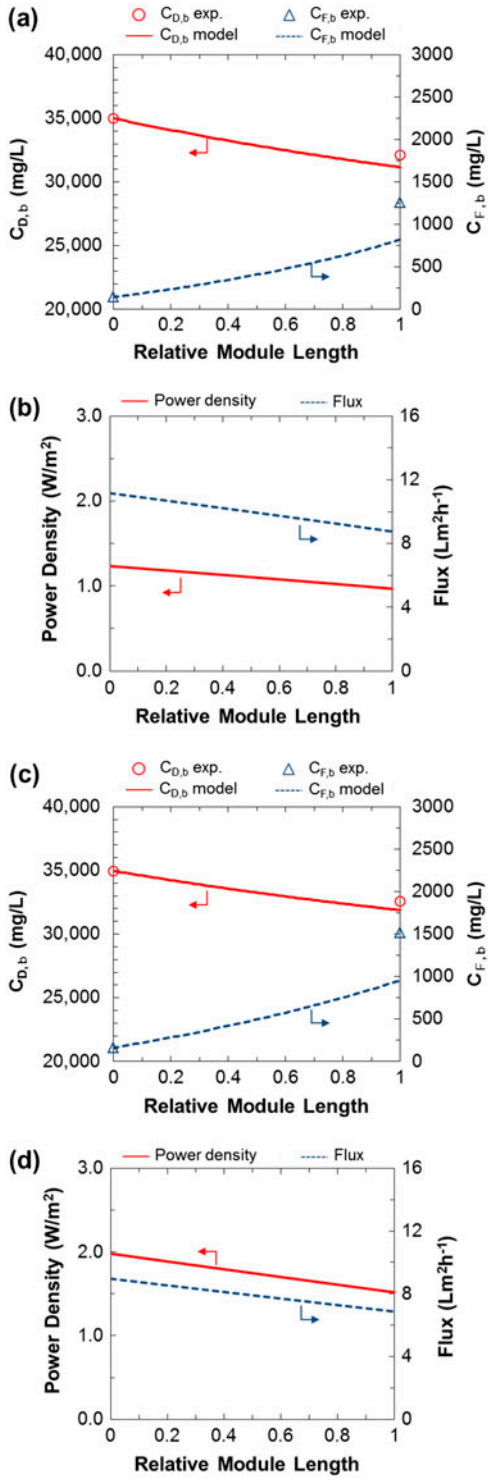

Fig. 7. Simulation results along the module direction.
Notes: Distribution of the concentration for draw and feed solutions at 4 bar (a) and 8 bar (c). Distribution of power density and water flux at 4 bar (b) and 8 bar (d). Open symbols in (a) and (d) represent experimental concentrations of the draw and feed solutions at inlet and outlet of the PRO module.

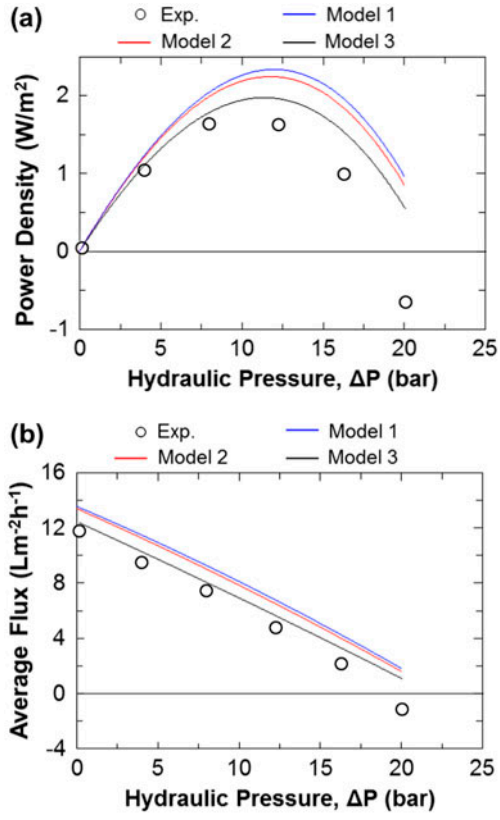

Fig. 8. Experimental and simulated power density (a) and water flux (b) for the PRO module.
Notes: Experimental conditions: The draw and feed solutions were 35,000 mg L^{-1} NaCl and tap water (140 mg L^{-1}), respectively. The inlet flow rates of draw and feed solutions were maintained at 25 and 7 LPM, respectively. Simulation condition: Model 1—draw concentration at 35,000 mg L^{-1}, feed concentration at 140 mg L^{-1}, and mass transfer coefficient 9.68×10^{-5} m s^{-1} (laboratory-scale test condition). Model 2—draw concentration at 35,000 mg L^{-1}, feed concentration at 140 mg L^{-1}, and mass transfer coefficient 4.67×10^{-5} m s^{-1} (module test condition). Model 3—updated values of draw and feed concentrations and mass transfer coefficient inside PRO module were applied.

performance using membrane transport properties. Model 3 estimated the maximum power density of 2.0 W m^{-2} at 11.3 bar of ΔP which is 0.23 W m^{-2} (13%) higher than the experiment result. However, model 3 overestimated for flux and power density as the hydraulic pressure was increased above 8 bar. The overestimation of model at high ΔP has been reported in previous laboratory-scale studies [17,24]. The results suggest membrane deformation for decrease of the PRO membrane performance at high hydraulic pressure difference. She et al. found severe membrane deformation when a net-type spacer was used for the feed channel compared to a tricot type spacer [17].

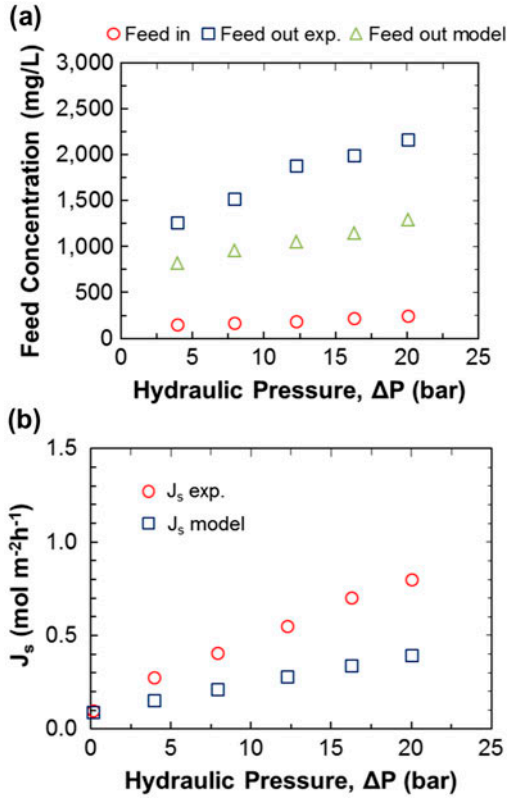

Fig. 9. Experimental and simulated concentration of feed solution (a) and reverse salt flux (b) for the PRO module as a function of hydraulic pressure difference (ΔP).
Note: Model 3 was used for the simulation data.

Kim et al. suggested a laboratory-test PRO cell design to minimize membrane deformation by the PRO channel of the laboratory-test cell [21]. The proposed PRO test cell could prevent membrane deformation by itself, and it could estimate the effect of the spacer on the PRO membrane performance. They found an increase of reverse salt flux with an increase of hydraulic pressure difference. In this study, model 3 also estimated an increase of the reverse salt flux (J_s) from 0.15 mol m^{-2} h^{-1} to 0.39 mol m^{-2} h^{-1} when hydraulic pressure increased from 4 to 20 bar. In the PRO process, less water flux at a higher hydraulic pressure difference could reduce the ECP and ICP effect. Consequently, an effective concentration difference across the membrane ($C_{D,m} - C_{F,m}$) could be increased at higher applied pressure. Meanwhile, the volume reduction effect of the feed solution for the increase of the concentration, which can be expressed as $Q_{F,\mathrm{in}}/(Q_{F,\mathrm{in}} - J_w A_m)$, decreases as hydraulic pressure difference increases. As shown in Fig. 9, the modeling results provided an increase of the outlet feed concentration as increasing hydraulic pressure difference. This indicates that the reverse salt flux of the investigated PRO membrane was more dominant in affecting the outlet feed concentration than the volume reduction effect of the feed solution. Although model 3 considered changes in the concentration of the draw solution and feed solutions along with the mass transport coefficient, the experimentally measured reverse salt flux was higher than the simulation results. Furthermore, the difference between the model and experimental values increased as increasing hydraulic pressure difference. This increase in reverse salt flux would negatively contribute to severe power density reduction at higher than 8 bar of ΔP. It could be attributed to membrane deformation or module defects at high hydraulic pressure differences. A PRO module can be operated at a higher applied hydraulic pressure difference when high-salinity water such as RO brine is used for the PRO process. Therefore, the development of the PRO membrane and module with high mechanical strength is required for higher power density.

4. Conclusions

Although the laboratory-scale experiment is useful in comparing the performance of different PRO membranes, there is a limitation when it comes to predicting the performance of the PRO module. We experimentally investigated the performance of a spiral-wound PRO membrane module and developed a model to predict the performance using membrane transport properties. The changes of draw and feed concentrations were observed in the PRO module; the concentration of draw solution was decreased due to dilution by water flux and the concentration of feed solution was increased due to volume reduction and reverse salt flux. The performance of the PRO module was predicted using a simulation considering changes of conditions including the draw and feed concentrations, and the mass transport coefficient inside the PRO module. Although simplified flow path in the module needs to be modified, our approach closely predicted the maximum power density of the PRO module. Under simulated conditions, the changes of the draw and feed concentrations dominantly affected the performance of the PRO module compared to ECP effect. This study could be used to predict effects of operational conditions including flow rates and concentrations of draw and feed solutions on power density of the PRO module. In addition, an increase of reverse salt permeability as increasing hydraulic pressure difference suggests a need for development of the PRO module with higher mechanical stability.

Acknowledgments

This research was supported by a grant (code 13IFIP-B065893-01) from the Industrial Facilities & Infrastructure Research Program funded by Ministry of Land, Infrastructure and Transport of Korean government and KHNP Central Research Institute, Korea Hydro & Nuclear Power Co., Ltd.

References

[1] K.L. Lee, R.W. Baker, H.K. Lonsdale, Membranes for power generation by pressure-retarded osmosis, J. Membr. Sci. 8 (1981) 141–171.
[2] N.Y. Yip, A. Tiraferri, W.A. Phillip, J.D. Schiffman, L.A. Hoover, Y.C. Kim, M. Elimelech, Thin-film composite pressure retarded osmosis membranes for sustainable power generation from salinity gradients, Environ. Sci. Technol. 45 (2011) 4360–4369.
[3] G.Z. Ramon, B.J. Feinberg, E.M.V. Hoek, Membrane-based production of salinity-gradient power, Energy Environ. Sci. 4 (2011) 4423–4434.
[4] N.Y. Yip, M. Elimelech, Performance limiting effects in power generation from salinity gradients by pressure retarded osmosis, Environ. Sci. Technol. 45 (2011) 10273–10282.
[5] F. La Mantia, M. Pasta, H.D. Deshazer, B.E. Logan, Y. Cui, Batteries for efficient energy extraction from a water salinity difference, Nano Lett. 11 (2011) 1810–1813.
[6] S.E. Skilhagen, J.E. Dugstad, R.J. Aaberg, Osmotic power—power production based on the osmotic pressure difference between waters with varying salt gradients, Desalination 220 (2008) 476–482.
[7] S. Loeb, F. Van Hessen, D. Shahaf, Production of energy from concentrated brines by pressure-retarded osmosis : II. Experimental results and projected energy costs, J. Membr. Sci. 1 (1976) 249–269.
[8] S. Chou, R. Wang, L. Shi, Q. She, C. Tang, A.G. Fane, Thin-film composite hollow fiber membranes for pressure retarded osmosis (PRO) process with high power density, J. Membr. Sci. 389 (2012) 25–33.
[9] A.P. Straub, N.Y. Yip, M. Elimelech, Raising the bar: Increased hydraulic pressure allows unprecedented high power densities in pressure-retarded osmosis, Environ. Sci. Technol. Lett. 1 (2013) 55–59.
[10] A. Achilli, A.E. Childress, Pressure retarded osmosis: From the vision of Sidney Loeb to the first prototype installation — Review, Desalination 261 (2010) 205–211.
[11] K. Gerstandt, K.V. Peinemann, S.E. Skilhagen, T. Thorsen, T. Holt, Membrane processes in energy supply for an osmotic power plant, Desalination 224 (2008) 64–70.
[12] M. Kurihara, M. Hanakawa, Mega-ton water system: Japanese national research and development project on seawater desalination and wastewater reclamation, Desalination 308 (2013) 131–137.
[13] Y.C. Kim, Y. Kim, D. Oh, K.H. Lee, Experimental investigation of a spiral-wound pressure-retarded osmosis membrane module for osmotic power generation, Environ. Sci. Technol. 47 (2013) 2966–2973.
[14] A. Efraty, Pressure retarded osmosis in closed circuit: A new technology for clean power generation without need of energy recovery, Desalin. Water Treat. 51 (2013) 7420–7430.
[15] A. Efraty, Closed circuit PRO series no 3: Status and prospects for PRO hydroelectric power generation from sea–river water like salinity gradients, Desalin. Water Treat. in press, doi: 10.1080/19443994.2015.1017321.
[16] A. Efraty, Closed circuit PRO series no 2: Performance projections for PRO membranes based on actual/ideal flux ratio of forward osmosis, Desalin. Water Treat. in press, doi: 10.1080/19443994.2015.1010275.
[17] Q. She, D. Hou, J. Liu, K.H. Tan, C.Y. Tang, Effect of feed spacer induced membrane deformation on the performance of pressure retarded osmosis (PRO): Implications for PRO process operation, J. Membr. Sci. 445 (2013) 170–182.
[18] Y. Xu, X. Peng, C.Y. Tang, Q.S. Fu, S. Nie, Effect of draw solution concentration and operating conditions on forward osmosis and pressure retarded osmosis performance in a spiral wound module, J. Membr. Sci. 348 (2010) 298–309.
[19] S. Phuntsho, S. Vigneswaran, J. Kandasamy, S. Hong, S. Lee, H.K. Shon, Influence of temperature and temperature difference in the performance of forward osmosis desalination process, J. Membr. Sci. 415–416 (2012) 734–744.
[20] N.Y. Yip, A. Tiraferri, W.A. Phillip, J.D. Schiffman, M. Elimelech, High performance thin-film composite forward osmosis membrane, Environ. Sci. Technol. 44 (2010) 3812–3818.
[21] Y.C. Kim, J.H. Lee, S.-J. Park, Novel crossflow membrane cell with asymmetric channels: Design and pressure-retarded osmosis performance test, J. Membr. Sci. 476 (2015) 76–86.
[22] S.-S. Hong, W. Ryoo, M.-S. Chun, S.O. Lee, G.-Y. Chung, Numerical studies on the pressure-retarded osmosis (PRO) system with the spiral wound module for power generation, Desalin. Water Treat. 52 (2013) 6333–6341.
[23] B. Gu, D.Y. Kim, J.H. Kim, D.R. Yang, Mathematical model of flat sheet membrane modules for FO process: Plate-and-frame module and spiral-wound module, J. Membr. Sci. 379 (2011) 403–415.
[24] Y.C. Kim, M. Elimelech, Adverse impact of feed channel spacers on the performance of pressure retarded osmosis, Environ. Sci. Technol. 46 (2012) 4673–4681.
[25] D.D. Anastasio, J.T. Arena, E.A. Cole, J.R. McCutcheon, Impact of temperature on power density in closed-loop pressure retarded osmosis for grid storage, J. Membr. Sci. 479 (2015) 240–245.
[26] Q. She, X. Jin, C.Y. Tang, Osmotic power production from salinity gradient resource by pressure retarded osmosis: Effects of operating conditions and reverse solute diffusion, J. Membr. Sci. 401–402 (2012) 262–273.
[27] F.-J. Fu, S.-P. Sun, S. Zhang, T.-S. Chung, Pressure retarded osmosis dual-layer hollow fiber membranes developed by co-casting method and ammonium persulfate (APS) treatment, J. Membr. Sci. 469 (2014) 488–498.
[28] Y.C. Kim, S.-J. Park, Experimental study of a 4040 spiral-wound forward-osmosis membrane module, Environ. Sci. Technol. 45 (2011) 7737–7745.
[29] K. Touati, F. Tadeo, T. Schiestel, Impact of temperature on power recovery in osmotic power production by pressure retarded osmosis, Energy Procedia 50 (2014) 960–969.